Volume 40
Number 5
May 2025
Pages 1125–1420

JAAS

Journal of Analytical Atomic Spectrometry

rsc.li/jaas

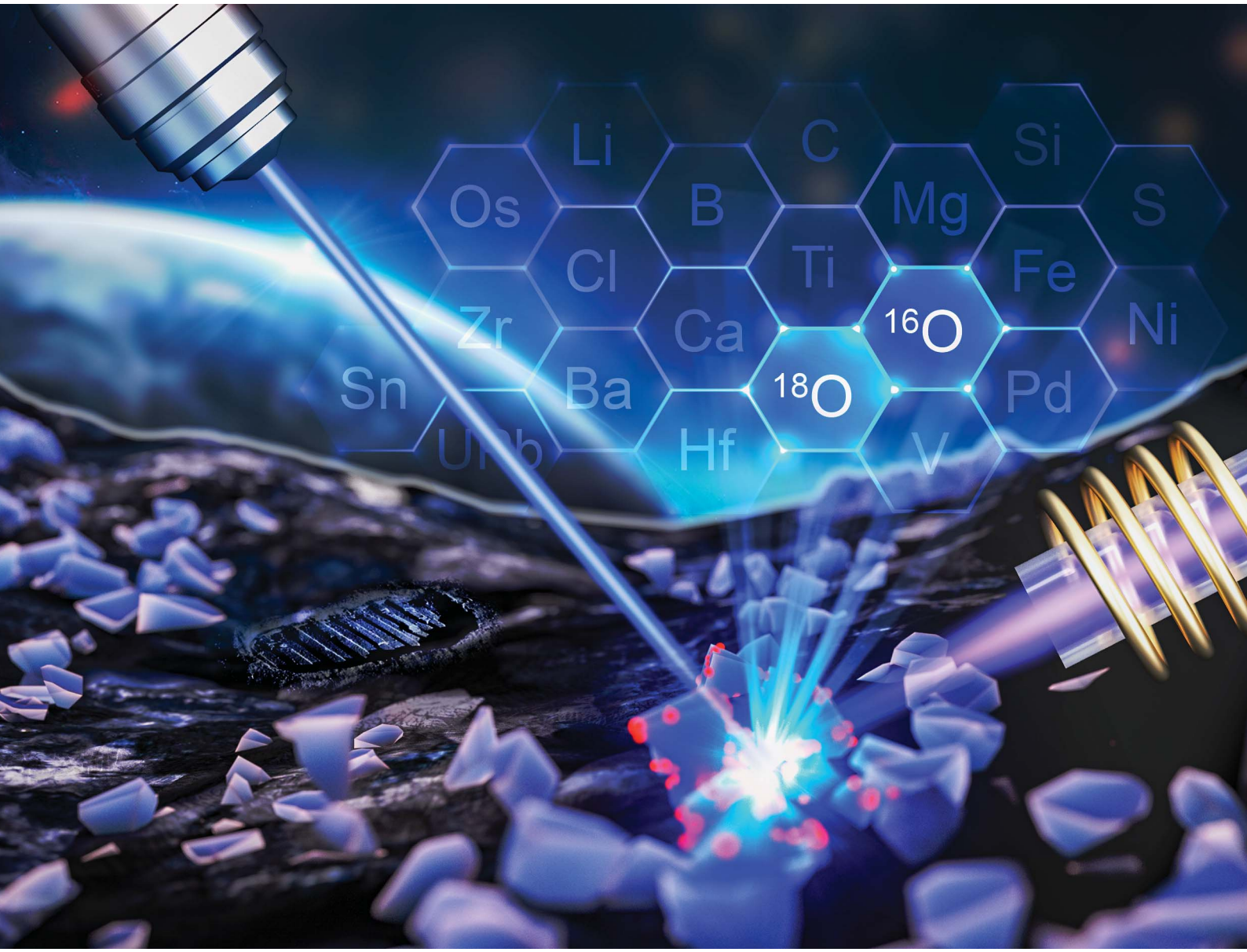

ISSN 0267-9477

ROYAL SOCIETY OF CHEMISTRY

PAPER

Jie Lin *et al.*

First attempt to determine oxygen isotopes in oxygen by MC-ICP-MS

JAAS

ROYAL SOCIETY OF CHEMISTRY

PAPER

View Article Online
View Journal | View Issue

Cite this: *J. Anal. At. Spectrom.*, 2025, **40**, 1192

First attempt to determine oxygen isotopes in oxygen by MC-ICP-MS

Zhenyi Liu, [a] Jie Lin, *[a] Xin Jiang,[a] Xi Zhu, [a] Wengui Liu,[a] Yongsheng Liu, [ab] Wen Zhang [a] and Zhaochu Hu [ac]

Oxygen is the key component of crustal and mantle rocks and fluids. The oxygen isotopic composition is a key tool to understand Earth's geological history and processes, such as continental formation, magmatic-hydrothermal processes, and crust–mantle interactions. The oxygen isotopic analysis is commonly implemented by Isotope Ratio Mass Spectrometry (IRMS) and Secondary Ion Mass Spectrometry (SIMS); however, its wide application is limited by the high cost and serious matrix effect. LA-MC-ICP-MS has been the method of choice for *in situ* isotopic analysis due to its relatively low cost, high analysis speed, high spatial resolution, and the low matrix effect. The determination of oxygen isotope using Ar-ICP has two limitations. Firstly, the exposure of Ar-ICP to the atmosphere may result in atmospheric interference, leading to an increase in the blank of oxygen isotopes and a reduction in the signal-to-blank (S/B) ratio. Secondly, the presence of doubly-charged Ar ions introduces interference that affects the accuracy of oxygen isotopic analysis. In order to investigate whether MC-ICP-MS can be used in the determination of oxygen isotopes, we attempt to use three approaches ($^{18}O^{16}O/^{16}O^{16}O$, $^{18}O/^{16}O$ and $^{18}O^{1}H_2/^{16}O^{1}H_2$) to determine oxygen isotopes in oxygen, and the applicability of three approaches is assessed based on interference, peak width, sensitivity, and stability. With our built methods, the obtained long-term productivity of $\delta^{18}O$ measured by $^{16}O^{18}O/^{16}O^{16}O$ was greater than 0.16‰ (2 SD), and the measured results for oxygen were consistent with those obtained by IRMS and MC-MIP-MS within the uncertainty limit. This demonstrates the feasibility of our method and also lays the foundation for the realization of *in situ* oxygen isotope analysis using LA-MC-ICP-MS.

Received 21st January 2025
Accepted 3rd February 2025

DOI: 10.1039/d5ja00025d

rsc.li/jaas

1. Introduction

Oxygen is a major component of crustal and mantle rocks and fluids and is the most abundant element in the silicate Earth. Oxygen isotopes are considered an effective means to study geological processes[1] and have been widely used in frontier scientific research fields, such as continental formation and evolution, early Earth history, magmatic-hydrothermal processes and metallogeny, crust–mantle composition and interactions, paleo-oceanic and paleoclimatic changes, and planetary geology and cosmogony.[2–14] Traditionally, two primary methods are commonly applied to analyze the oxygen isotopes: Isotope Ratio Mass Spectrometry (IRMS) and Secondary Ion Mass Spectrometry (SIMS).[15–22]

The IRMS analysis method is a bulk analysis method for oxygen isotopes and includes the conventional BrF_5 method[23–25] and laser microprobe BrF_5 method.[26–29] The conventional BrF_5 method is a reliable technique for accurate oxygen isotope analysis of whole rocks and individual minerals, including silicates, phosphates, and sulfates. It typically requires a sample volume of 5–15 mg to react with excess BrF_5 in nickel reaction tubes at specified temperatures and durations. Although the analytical accuracy of this method can reach ±0.05–0.1‰, certain refractory minerals demand higher temperatures and a longer duration for sample melting. For instance, garnet and olivine necessitate a high temperature of 690 °C maintained for 12 hours.[23,25] In contrast, the laser microprobe BrF_5 method replaces external heating of nickel tubes with direct laser heating, which reaches a high temperature of approximately 2000 K. This innovation enables oxygen isotopic analysis of some refractory minerals, significantly reduces sample volume requirements to less than 100 μg and also maintains good analytical precision (±0.05–0.1‰).[29–31] However, the thermal effects occurring during the laser heating process can lead to significant isotopic fractionation, thereby influencing the precision and accuracy of the analysis.[32–36] Furthermore, both methods require the use of strong corrosive reagents, posing potential safety hazards. Compared with the bulk analysis method by IRMS, SIMS can be capable of performing *in situ* microanalysis of oxygen isotopes, which can offer the high

[a]*State Key Laboratory of Geological Processes and Mineral Resources, School of Earth Sciences, China University of Geosciences, Wuhan 430074, China. E-mail: linjie@cug.edu.cn*

[b]*Yangtze University, Jingzhou, 434023, China*

[c]*Faculty of Materials Science and Chemistry, China University of Geosciences, Wuhan 430074, China*

spatial resolution of 5–20 μm beam spot and 1–2 μm depth with high analytical precision (better than 0.4‰).[37] However, the analytical results obtained by SIMS are susceptible to a severe matrix effect, *i.e.*, the difference in chemical compositions and morphological characteristics of the standard and sample.[21,22,37–39] Additionally, the high maintenance and operation cost has also constrained the widespread use of SIMS for *in situ* analysis of oxygen isotopes,[15,18,20–22,40] and it has only been applied to the *in situ* oxygen isotopic analysis of the simple single mineral (*e.g.*, pyroxene, zircon barite and olivine).[22,40–43] In addition, the high sample preparation requirements for SIMS, which necessitate that samples be compatible with high vacuum conditions, can significantly limit its applicability, especially when dealing with loosely structured and volatile samples.[44] In particular, with the development of modern geosciences, more and more studies have shown that *in situ* oxygen isotope analysis plays a key role in revealing some major geoscientific issues. For example, *in situ* microanalysis of oxygen isotopes from ancient zircons, targeting pristine domains within individual crystals to avoid later alteration, indicated the existence of a hydrosphere and water–rock interaction on Earth before >4.1 Ga;[45,46] oxygen isotopic composition in diamonds and their inclusions, specifically the pristine domains within the crystals, illustrated the presence of cryogenically altered oceanic crust in deep continental areas.[5,6,47] High-resolution paleoclimate records obtained through *in situ* microanalysis of oxygen isotopes can elucidate the relationships between paleoclimate changes, biological explosions, and mass extinctions.[3,7,48] Therefore, it is essential to develop new techniques for *in situ* oxygen isotope analysis with high spatial resolution, high precision, and high accuracy.

Multi-Collector Inductively Coupled Plasma Mass Spectrometry (MC-ICP-MS) has become the method of choice for analyzing the isotopic composition by virtue of its advantages such as high precision and accuracy, fast analysis speed, a weak matrix effect and low operating cost.[49–54] In particular, since the ICP operates under atmospheric pressure conditions, it can be flexibly switched among multiple sample introduction methods (traditional nebulizers and spray chambers, membrane desolvation,[55,56] laser ablation system[49,57–60] as well as the direct introduction of gaseous samples.[61,62]). Among them, LA-MC-ICP-MS, which combines the advantages of *in situ* sample introduction by a laser ablation system and the high-precision isotopic determination by MC-ICP-MS, has already accurately analyzed more than 23 isotopes.[51] In particular, the successful determination of high-ionization-energy isotopes (*e.g.*, C (10.4 eV),[49] S (10.0 eV)[63] and Cl (12.97 eV)[50]) using LA-MC-ICP-MS has encouraged us to explore the *in situ* microanalysis of oxygen isotopes. Compared with C, S and Cl, O has a higher ionization energy of 13.6 eV, although it is lower than that of Ar (15.6 eV). Oxygen can be ionized in argon inductively coupled plasma (Ar-ICP), but its ionization efficiency is only about 0.1% based on the Saha equation.[64] Moreover, two additional challenges exist. First of all, the Ar-ICP is exposed to the atmosphere, and the determination of oxygen isotopes can be interfered with by the oxygen components in the air. Second, as Ar is used as the plasma gas, the precision and accuracy of oxygen isotopic analysis can be severely impacted by the interference from $^{36}Ar^{2+}$. Consequently, in view of the inherent characteristics of Ar-ICP, no attempts have been made to employ MC-ICP-MS for oxygen isotopic analysis. Therefore, it is necessary to first explore whether the determination of the oxygen isotopic composition can be achieved by MC-ICP-MS, which is the prerequisite for discussing the applicability of LA-MC-ICP-MS in analyzing the oxygen isotope.

In this study, with the application of the simplest oxygen gas as the analyzing sample, we attempted to determine the oxygen isotope composition of oxygen using MC-ICP-MS by employing three methods, $^{18}O/^{16}O$, $^{16}O^{18}O/^{16}O^{16}O$, and $^{18}O^{1}H_2/^{16}O^{1}H_2$. The ionization efficiency of oxygen in Ar-ICP was assessed by evaluating the sensitivity of all three analytes. Meanwhile, interference and the peak width were analyzed and quantified to assess the impacts of atmospheric oxygen components and argon. From the perspective of isotopic analysis, we evaluated the isotopic analytical reproducibility, the stability of oxygen isotope ratios, as well as the measurement accuracy. Through systematic investigation, $^{18}O/^{16}O$ and $^{16}O^{18}O/^{16}O^{16}O$ were selected for oxygen isotopic analysis. Furthermore, the accuracy of the established method was evaluated by comparing the obtained results with those acquired from MAT 253 and MC-MIP-MS. This demonstrated the feasibility of our method and laid the foundation for the realization of *in situ* oxygen isotope analysis using LA-MC-ICP-MS.

2. Experimental design

A double-focusing Neptune Plus MC-ICP-MS system (Thermo Fisher Scientific, Germany), equipped with seven ion counters and nine Faraday cups, was used at the State Key Laboratory of Geological Processes and Mineral Resources, China University of Geosciences in Wuhan (GPMR). In our experiment, $^{18}O/^{16}O$, $^{18}O^{16}O/^{16}O^{16}O$ and $^{18}O^{1}H_2/^{16}O^{1}H_2$ were used for oxygen isotopic analysis, in which the high-mass particles (^{18}O, $^{18}O^{16}O$, and $^{18}O^{1}H_2$) were measured on an H4 cup and low-mass particles (^{16}O, $^{16}O^{16}O$, and $^{16}O^{1}H_2$) were measured on an L4 cup, and "dummy" masses (m/z = 16.990, 33.030, 19.042) were measured on the center cup. The H4 Faraday cup was equipped with a 10^{11} Ω resistor, whereas the L4 Faraday cup was equipped with a 3×10^{9} Ω resistor due to the high blank intensity of $^{16}O^{+}$ and $(^{16}O^{16}O)^{+}$. To eliminate the interference of $^{36}Ar^{2+}$ in the determination of $^{18}O^{+}$ and because two adjacent Faraday cups cannot receive both signals simultaneously (the mass difference between $^{18}O^{+}$ and $^{36}Ar^{2+}$ is 0.0154 amu), we built a sub-cup configuration for the determination of $^{36}Ar^{2+}$, wherein a Faraday cup H4 was used, and a "dummy" mass (m/z = 16.975) was measured in the center cup. In addition to $^{36}Ar^{2+}$, there are also interferences from $^{40}Ar^{2+}$, $^{32}S^{+}$ and $^{34}S^{+}$ in oxygen isotope measurements, thus the high mass resolution ($m/\Delta m$ = 5500) was applied to eliminate related polyatomic ion interference. Two tanks of oxygen (>99.999%) were used as the bracketing standard and sample, respectively. The O_2 (0.1–2 mL min^{-1}) and He sweeping gas flows were controlled using a mass flow meter (MFC). High-purity He (99.999%) was used as a sweeping gas to clean residual oxygen

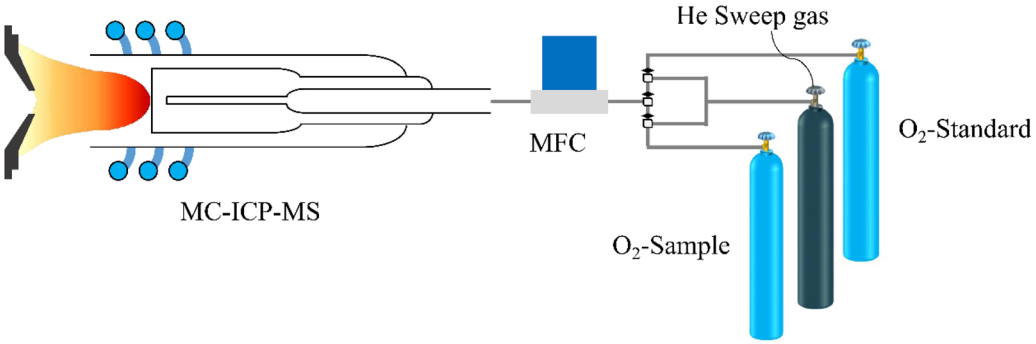

Fig. 1 Schematic of the MC-ICP-MS inlet system in the oxygen isotopic analysis.

from pipelines. The schematic of the MC-ICP-MS inlet system in the oxygen isotopic analysis can be seen in Fig. 1.

The oxygen isotope composition of the oxygen was determined using the sample-standard bracketing method (SSB), a technique designed to correct for mass bias and instrumental drift during isotopic analysis. To minimize the influence of blank on the isotopic measurements,[65] the on-peak blank was analyzed prior to each sample and standard measurement, utilizing a block of 15 cycles with an integration time of 4.194 seconds. Analysis of each sample and standard was conducted by one block of 30 cycles, with the integration time of 4.194 s. A repeated analytical sequence of "blank, O_2-std, blank, O_2-sample, blank, O_2-std, blank…" was conducted. And offline calculations of the blank and analyte signals, time-drift correction, and isotopic analysis calibration were performed using Iso-Compass software.[66] To verify the accuracy of the proposed method, an IRMS (Thermo Scientific™ MAT253 Plus™) at GPMR was used as a comparative method to analyze oxygen isotopes, and the instrumental operating parameters for MC-ICP-MS and IRMS are summarized in Table 1. The oxygen isotopes of the sample are expressed as $\delta^{18}O$, which can be calculated using eqn (1)–(4).

$$r = ({}^{16}O{}^{18}O)^+/({}^{16}O{}^{16}O)^+ \quad (1)$$

$$r' = {}^{18}O/{}^{16}O = r/(2 + r) \quad (2)$$

$$r' = {}^{18}O/{}^{16}O = ({}^{18}O{}^{1}H{}^{1}H)^+/({}^{16}O{}^{1}H{}^{1}H)^+ \quad (3)$$

$$\delta^{18}O = \left(r'_{\text{sample}}/r'^{-1}_{\text{std}}\right) \times 1000 \quad (4)$$

where r is the measured ${}^{16}O{}^{18}O/{}^{16}O{}^{16}O$ ratio. r' is the measured ${}^{18}O/{}^{16}O$ ratio (when ${}^{18}O/{}^{16}O$ was measured) or the ${}^{18}O/{}^{16}O$ ratio when converted from ${}^{16}O{}^{18}O/{}^{16}O{}^{16}O$ (when ${}^{16}O{}^{18}O/{}^{16}O{}^{16}O$ was measured) or the ${}^{18}O/{}^{16}O$ ratio when converted from ${}^{18}O{}^{1}H{}^{1}H/{}^{16}O{}^{1}H{}^{1}H$ (when ${}^{18}O{}^{1}H{}^{1}H/{}^{16}O{}^{1}H{}^{1}H$ was measured), r'_{sample} is the measured ${}^{18}O/{}^{16}O$ ratio of sample oxygen, and r'_{std} is the measured ${}^{18}O/{}^{16}O$ ratio of standard oxygen. $\delta^{18}O$ is the oxygen composition of the analyzed sample.

In our experiment, we integrated the existing oxygen isotopic analysis methods of SIMS, which determines negative ions such as ${}^{18}O^-/{}^{16}O^-$, as well as IRMS, which analyzes positive oxygen molecules like ${}^{16}O{}^{18}O^+/{}^{16}O{}^{16}O^+$, and combined the determination methods of other isotopes by MC-ICP-MS, including positive ions like ${}^{13}C^+/{}^{12}C^+$, ${}^{32}S^+/{}^{34}S^+$, and ${}^{37}Cl^+/{}^{35}Cl^+$. Based on these, a comprehensive evaluation of three possible methods (${}^{18}O/{}^{16}O$, ${}^{18}O{}^{16}O/{}^{16}O{}^{16}O$ and ${}^{18}O{}^{1}H_2/{}^{16}O{}^{1}H_2$) was conducted to explore the feasibility of using MC-ICP-MS for oxygen isotopic analysis.

3. Results and discussion

Given that oxygen isotopic analysis *via* MC-ICP-MS has never been explored before, we referred to the determination methods of other isotopes using MC-ICP-MS (determination of positive ions, *e.g.*, ${}^{13}C^+/{}^{12}C^+$,[49] ${}^{32}S^+/{}^{34}S^+$,[63,67] and ${}^{37}Cl^+/{}^{35}Cl^+$)[50] as well as SIMS (determination of negative ions, ${}^{18}O^-/{}^{16}O^-$)[22] and IRMS (determination of positive oxygen molecules, ${}^{16}O{}^{18}O^+/{}^{16}O{}^{16}O^+$).[68] Taking into account the high ionization capacity of ICP as well as the lens parameter in our instrument (with the extraction lens set at −2000 V), we opted to select ${}^{18}O^+$–${}^{16}O^+$ and ${}^{16}O{}^{18}O^+$–${}^{16}O{}^{16}O^+$ for oxygen isotopic analysis. Additionally, during the process of scanning the blank, we also detected H_2O^+. Hence, currently, there are three analytes available for oxygen isotopic analysis. To explore the feasibility of MC-ICP-MS to determine oxygen isotopes, a comprehensive evaluation of three possible methods was conducted, including the interference, sensitivity, dynamic linear range, stability of oxygen isotope ratios, analytical precision and accuracy of oxygen isotope ratios.

3.1 Interference on oxygen ions

The peak shapes of ${}^{18}O$–${}^{16}O$, ${}^{16}O{}^{18}O$–${}^{16}O{}^{16}O$ and ${}^{18}O{}^{1}H_2$–${}^{16}O{}^{1}H_2$ as well as the related interferences are scanned at an O_2 flow rate of 0 mL min^{-1} with a high mass resolution ($m/\Delta m = 5000$) (Fig. 2). For the measurement of ${}^{18}O/{}^{16}O$, ${}^{16}O{}^{18}O/{}^{16}O{}^{16}O$, and ${}^{18}O{}^{1}H_2/{}^{16}O{}^{1}H_2$, the main interferences are listed in Table 2. It can be seen that the determination of oxygen isotopes is susceptible to the interference of the plasma gas (Ar^{2+}) (Fig. 2b and e), S blank (Fig. 2c) and the atmosphere (O–H related interference) (Fig. 2a and f). Therefore, it is necessary to select the appropriate peak center to avoid the interference and obtain the true oxygen signal intensity for oxygen isotope determination.

In terms of ${}^{18}O$–${}^{16}O$, ${}^{36}Ar^{2+}$ and ${}^{16}O{}^{1}H_2{}^+$ are two main interferences. The doubly-charged interference of ${}^{36}Ar^{2+}$ is located

Table 1 Summary of the operating parameters for MC-ICP-MS

Instruments	Analyzed method	Operating conditions		
Neptune Plus MC-MS system				
Cup configuration	$^{18}O^{16}O/^{16}O^{16}O$	L4	C	H4
		$^{16}O^{16}O$	33.03	$^{16}O^{18}O$
	$^{18}O^{1}H^{1}H/^{16}O^{1}H^{1}H$	$^{16}O^{1}H^{1}H$	19.042	$^{18}O^{1}H^{1}H$
	$^{18}O/^{16}O$	^{16}O	16.990	^{18}O
Sub-cup configuration	$^{36}Ar^{2+}$		16.975	$^{36}Ar^{2+}$
Resistor of the Faraday cup		3×10^{9} Ω	10^{11} Ω	10^{11} Ω
Cool gas flow rate		15 L min^{-1}		
Aux gas flow rate		0.95 L min^{-1}		
Sample gas flow rate		1.12–1.45 L min^{-1}		
RF power		1050 W		
Guard electrode (GE)		On		
Extraction		−2000 V		
Focus		−676 V		
X-Defl		0.27 V		
Y-Defl		−3.48 V		
Shape		248 V		
Rot quad 1		0.01 V		
Source offset		−1.00 V		
Foc quad 1		−19.89 V		
Rot quad 2		0.00 V		
Focus offset		50.00 V		
Matsuda plate		0.01 V		
Focus quad		−8.00 V		
Dispersion quad		−1.00 V		
Interface cones		Jet sample cone + X skimmer cone		
Mass resolution		High ($m/\Delta m = 5500$)		
Block × cycle		1 × 30 (sample); 1 × 15 (blank)		
Integration time		4.194 s		

MAT253 Plus IRMS				
Cup configuration	$^{18}O^{16}O/^{16}O^{16}O$	C1	C2	C3
		$^{16}O^{16}O$	$^{16}O^{17}O$	$^{16}O^{18}O$
Resistor of the Faraday cup		3×10^{8} Ω	3×10^{11} Ω	1×10^{11} Ω
High voltage		9.450 KV		
Emission		1.2 mA		
Electron energy		108.926 V		
Trap		22.6 V		

on the low-mass side and the polyatomic ionic interference of $^{16}O^{1}H_2^{+}$ is located on the high-mass side. The interference of $^{16}O^{1}H_2^{+}$ on $^{18}O^{+}$ could be isolated as the mass center of the peak was chosen at the mass side of 16.990 with the high mass resolution (Fig. 2a and b). And for $^{36}Ar^{2+}$ (the mass difference between $^{18}O^{+}$ and $^{36}Ar^{2+}$ is 0.0154 amu, and two nearby Faraday cups cannot receive both signals at the same time), a sub-cup configuration was built, and the $^{36}Ar^{2+}$ signal can be directly acquired through peak jumping and deducted accurately. As for $^{16}O^{18}O$–$^{16}O^{16}O$, $^{32}S^{+}$ and $^{34}S^{+}$ are two main interferences, and fortunately both interferences are located on the low-mass side; thus, a mass center of 33.03 can be selected to avoid the interferences of $^{32}S^{+}$ and $^{34}S^{+}$ (Fig. 2c and d). For the determination of $^{18}O^{1}H_2$–$^{16}O^{1}H_2$, the main interferences are $^{36}Ar^{2+}$, $^{18}O^{+}$ and $^{40}Ar^{2+}$. Three interferences are all located on the low mass side, and a mass center of 19.042 was selected to avoid the interferences. Notably, the applied peak width of $^{16}O^{18}O/^{16}O^{16}O$ was approximately 0.015 amu (Fig. 2f), whereas those of $^{18}O/^{16}O$ and $^{18}O^{1}H_2/^{16}O^{1}H_2$ were 0.008 amu (Fig. 2b and d). Therefore, $^{16}O^{18}O/^{16}O^{16}O$ was estimated to be the preferred method in view of the peak width of the mass shoulder, which is crucial for accurate isotope measurement as it allows for better resolution and less interference from adjacent peaks.[69,70]

3.2 Sensitivity and dynamic linear range of oxygen ions

The Saha equation predicts a low ionization rate (approximately 0.1%) for oxygen in an Ar-ICP,[64] making high sensitivity a critical factor for achieving precise and accurate oxygen isotopic analysis. Besides, as the Ar-ICP is exposed to the atmosphere, the oxygen components in air generate a significantly high oxygen blank during isotopic analysis, which affects the accuracy of oxygen isotope measurements. Consequently, a comprehensive assessment of the sensitivity, blank levels, and signal-to-blank (S/B) ratios of the two methods is essential to ascertain their influence on the reliability of isotopic analysis.

The blank and sensitivity (sensitivity was obtained by the ratio of net signal intensity and oxygen gas flow rate) of ^{16}O and

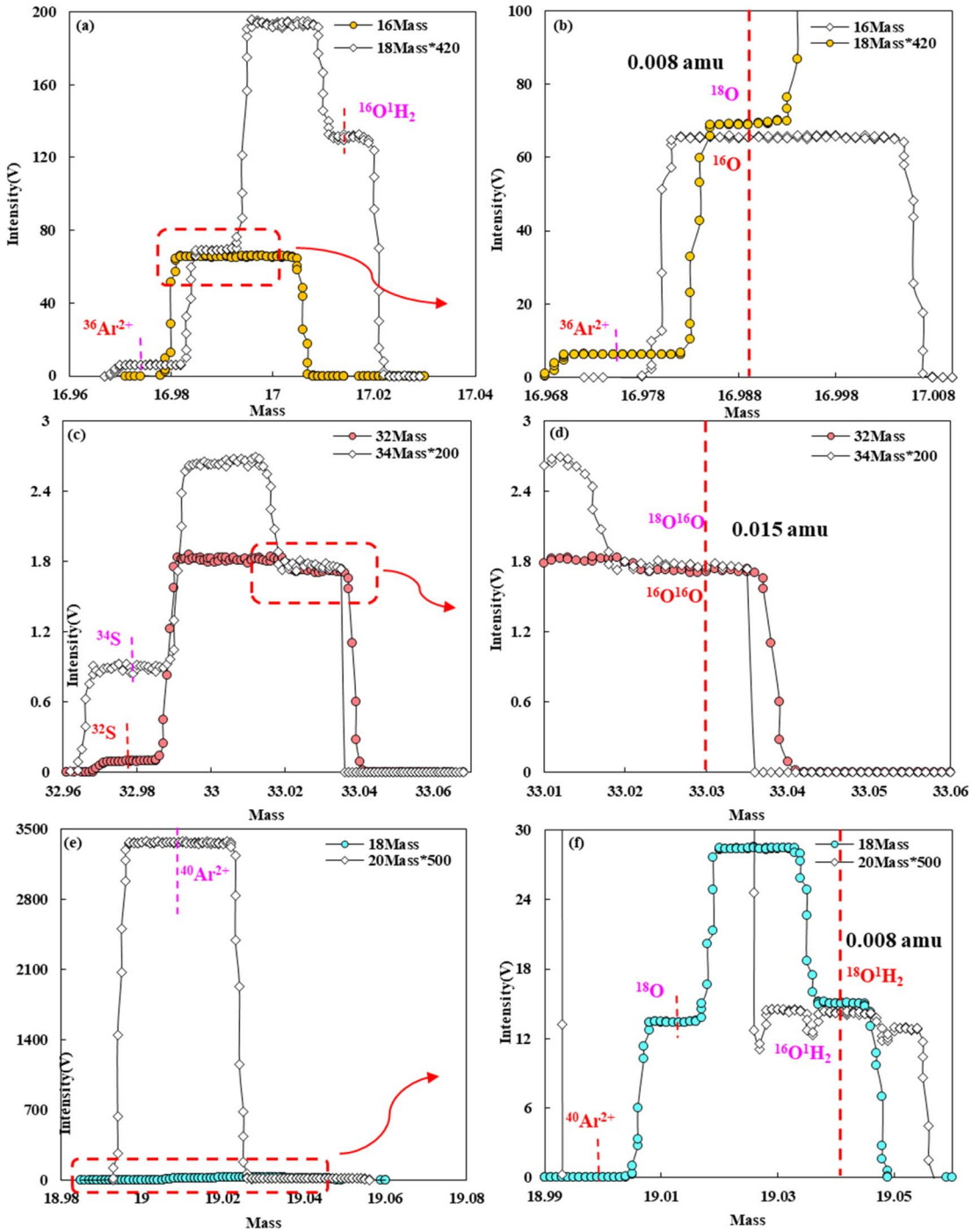

Fig. 2 Peak shapes of $^{16}O^{+}$–$^{18}O^{+}$ (a), $(^{16}O^{16}O)^{+}$–$(^{16}O^{18}O)^{+}$ (c) and $(^{16}O^{1}H^{1}H)^{+}$–$(^{18}O^{1}H^{1}H)^{+}$ (e) with high mass resolution in MC-ICP-MS. In the legend of "18Mass × 420", "34Mass × 200" and "20Mass × 500", 420-, 200- and 500-folds were used to obtain the signal intensities of 18Mass, 34Mass and 20Mass, consistent with those of 16Mass, 18Mass and 32Mass to check the simultaneous collection of the two peaks. Part figures (a, c and e) in the dashed box are enlarged to locate more suitable peak centers (mass = 16.990, 33.030 and 19.042) (b, d and f).

$^{16}O^{16}O$ were examined as the O_2 flow rate increased from 0 to 2 mL min^{-1} (Fig. 3). For the measurement of $^{18}O/^{16}O$, the ^{16}O blank can be as high as 64 V, which may be due to the exposure of the ICP in the atmosphere.[71] At the sample gas flow rate of 1.29 L min^{-1} and RF power of 1050 W, the ^{16}O intensity increased as the O_2 flow rate increased from 0 to 0.5 mL min^{-1}, as demonstrated by the linear function of intensity *versus* the O_2 flow rate. The slope of the linear regression relationship was 2430, which can be demonstrated as sensitivity (*i.e.*, ~2430 V mL^{-1} min^{-1}). However, beyond this flow rate, the ^{16}O signal intensity will exceed the Faraday cup's threshold of 1666 V when using a 3×10^9 Ω resistor. Thus, the applied O_2 flow rate was 0.5 mL min^{-1}, and the S/B ratio of this method was 22.49. For the analyzed method of $^{16}O^{18}O/^{16}O^{16}O$, at the sample gas flow rate

Table 2 Data for analyzed isotopes, related interfering ions, and mass resolutions

Analyzed isotopes	Mass	Interfering ions	Mass	Required mass resolution	Peak width (amu)	Blank (V)	Signal-to-blank ratio	Sensitivity (V ml^{-1} min^{-1})
^{16}O	15.9949	$^{14}N^{1}H_{2}^{+}$	16.0187	672	0.008	65.80 (^{16}O)	22.49	2430
^{18}O	17.9992	$^{36}Ar^{2+}$	17.9838	1170				
		$^{16}O^{1}H_{2}^{+}$	18.0106	1578				
		$^{14}N^{1}H_{4}^{+}$	18.0344	511				
$^{16}O^{16}O$	31.9898	$^{32}S^{+}$	31.9721	1807	0.015	0.80 ($^{16}O^{16}O$)	1585	719
		$^{14}N^{18}O$	32.0022	2579				
		$^{14}N^{16}O^{1}H_{2}^{+}$	32.0136	1344				
$^{16}O^{18}O$	33.9941	$^{34}S^{+}$	33.9679	1297				
		$^{16}O^{16}O^{1}H_{2}^{+}$	34.0055	2981				
$^{16}O^{1}H_{2}$	18.0107	$^{36}Ar^{2+}$	17.9838	670	0.008	0.43 ($^{16}O^{1}H_{2}$)	32.39	7
		$^{18}O^{+}$	17.9992	1566				
		$^{14}N^{1}H_{4}^{+}$	18.0344	760				
$^{18}O^{1}H_{2}$	20.0132	$^{40}Ar^{2+}$	19.9812	625				

of 1.254 L min^{-1} and RF power of 1050 W, the $^{16}O^{16}O$ intensity increased linearly with the O_2 flow rate of up to 1.8 mL min^{-1}, beyond which a nonlinear relationship was observed. The slopes of the linear regression relationship were 718, which can be demonstrated as the sensitivity (*i.e.*, ~680 V mL^{-1} min^{-1}). This nonlinearity may stem from incomplete ionization of the O_2 sample under the current conditions.[72,73] To reduce the isotopic fractionation and obtain the best precision, the O_2 flow rate of 1.6 mL min^{-1} was selected for the measurement of $^{18}O^{16}O/^{16}O^{16}O$ with the S/B ratio of this method being 1585.25.

In order to select an appropriate analysis method, we proceeded with two perspectives: sensitivity and S/B ratio. Based on our experiment, $^{18}O/^{16}O$ is the preferred option in terms of sensitivity (2430 V ml^{-1} min^{-1}). This observation is somewhat surprising, the first ionization energy of an O atom (13.62 eV) is higher than that of $^{16}O^{16}O$ (12.07 eV), which suggests that the sensitivity of $^{16}O^{16}O$ should be greater than that of ^{16}O theoretically. The high sensitivity of ^{16}O may be attributed to the high gas temperature of the ICP ion source, which can lead to the dissociation of most O_2 into O atoms, leaving a small fraction of undissociated O_2 molecules. However, from the perspective of S/B ratio, the S/N ratio of ^{16}O (22.49) was 750 times lower than that of $^{16}O^{16}O$ (1585.25). Therefore, when considering the two aspects of sensitivity and S/N ratio, the choices of optimal methods to be tested are contradictory. To explore the interaction between the S/B ratio and signal intensity in isotopic analysis, a simulation experiment was performed. Two simulated datasets were created: one with low signal intensity but high S/B ratios and the other with high signal intensity but low S/B ratios, while keeping the isotope composition of blank (−12‰) and sample (0.5‰) constant. For each dataset, the blank intensity was fixed (0.005 V *vs.* 0.2 V), and the signal intensity (1–8 V *vs.* 21–28 V) was varied to achieve different S/B ratios (200–1600 *vs.* 105–140). Isotopic compositions were calculated without blank correction, and the relative error (RE) between the calculated and true sample compositions was assessed. Fig. 4a and b shows that for the group with a high signal intensity but low S/B ratio, the blank intensity had a more significant impact on isotopic measurements. For example, even at a signal intensity of 28 V with a low S/B ratio (140), the effect of blank on isotopic composition was considerable, with an RE as high as −29.94%. Conversely, for the high S/B ratio

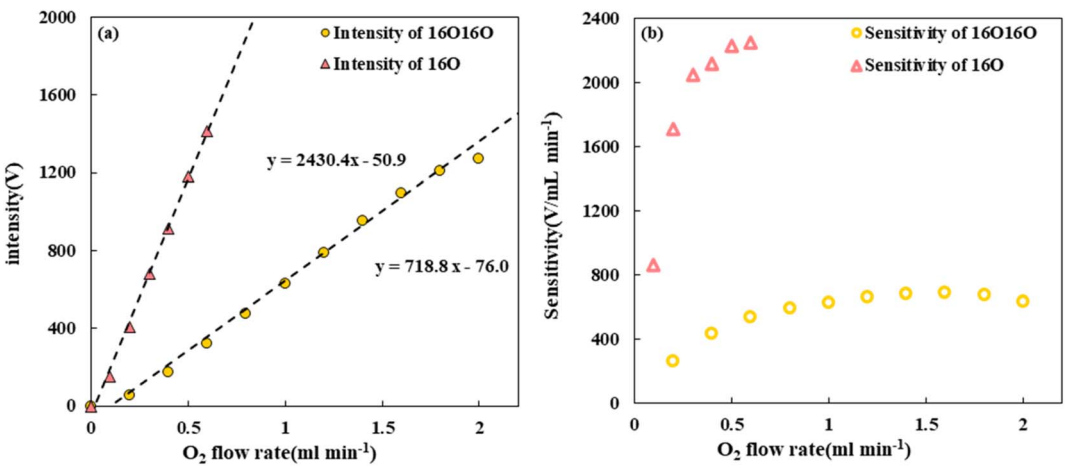

Fig. 3 Relationship between the O_2 flow rate and the signal intensity (a) as well as the sensitivity (b) of ^{16}O and ($^{16}O^{16}O$).

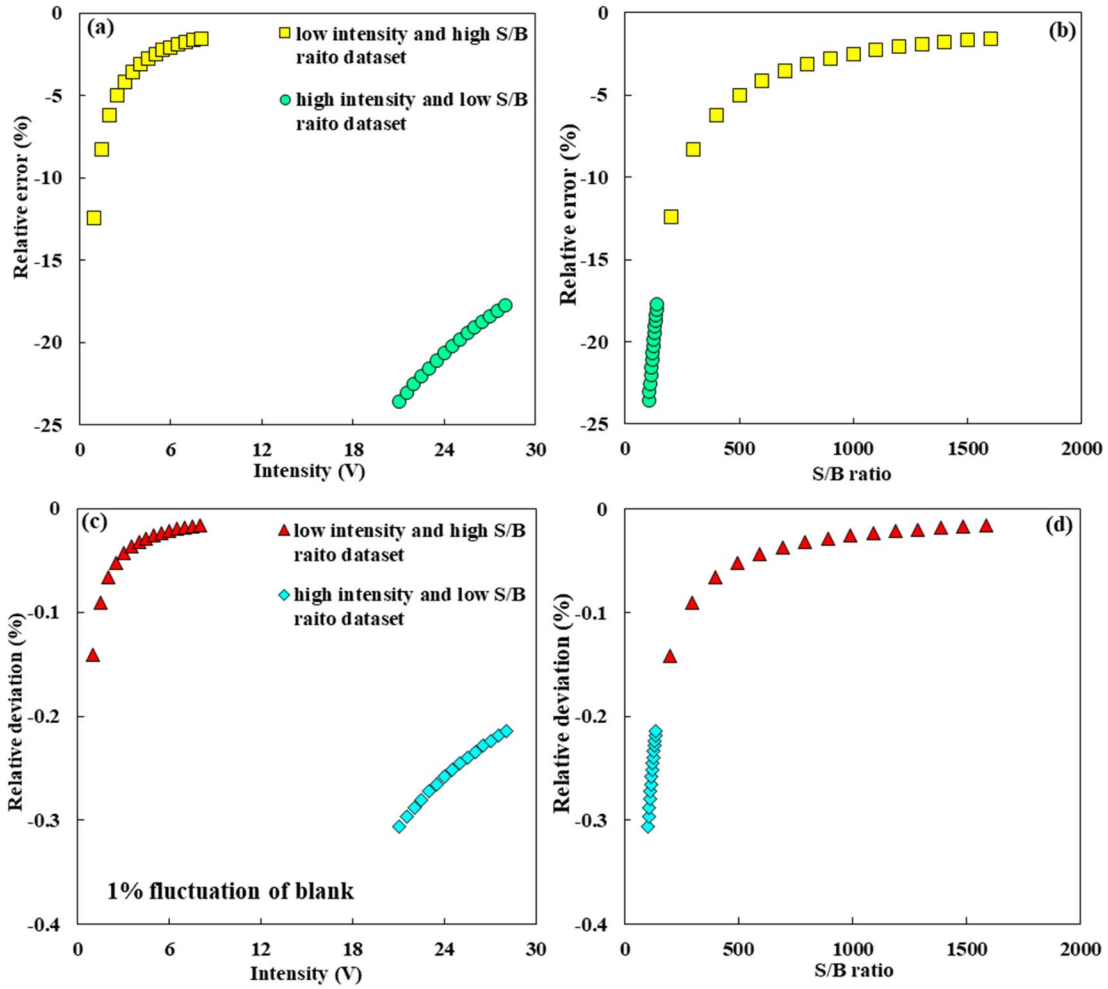

Fig. 4 (a) and (b) Relationship between the signal intensity, S/B ratio and relative error of the two simulated datasets; the relative error was calculated between the calculated and true sample compositions. (c) and (d) Relationship between the signal intensity, S/B ratio and relative deviation of the two simulated datasets; the relative deviation was assessed by the sample composition before and after 1% blank fluctuation.

group, where the S/B ratio reached 1000 at a low signal intensity of 5 V, the effect of blank on isotopic composition (RE) was less than 2.5%. Here, despite an 82.1% reduction in signal intensity (from 28 V to 5 V) compared to the high signal intensity group, the effect of the blank can be reduced by 91.6%. Fig. 4c and d further examines the effect of 1% fluctuation in blank intensity. The results indicated that such fluctuations affected the high signal intensity but a low S/B ratio group more than the low signal intensity but a high S/B ratio group. At an S/B ratio of 1000, a 1% blank fluctuation caused only a 0.03% change in the calculated isotopic composition at a signal intensity of 5 V. However, for the high signal intensity group, the same fluctuation led to a 1.01% change in isotopic composition at 28 V due to the low S/B ratio (140).

These simulations highlight the crucial balance between the signal intensity and S/B ratio in isotope analysis. The higher S/B ratios enhance the accuracy of isotope ratio measurements by reducing blank, which is especially vital in laser-based *in situ* microanalysis of samples with low elemental concentrations and low signal intensities. Achieving high S/B ratios is essential for reliable measurements in such scenarios. In summary, accurate determination of isotopic compositions necessitates not only sufficient signal intensity but also optimized S/B ratios to ensure high precision and accuracy across a variety of analytical conditions. In this context, $^{18}O^{16}O/^{16}O^{16}O$, which exhibits a higher S/B ratio, is more suitable as the analyte of analysis. Additionally, the peak width of $^{18}O^{16}O/^{16}O^{16}O$ (0.015 amu) is wider than that of $^{18}O/^{16}O$ (0.008 amu) and the blank intensity of $^{16}O^{16}O$ (0.8 V) is lower than that of ^{16}O (65.8 V). Therefore, considering the S/B ratio, peak width and blank, the use of $^{18}O^{16}O/^{16}O^{16}O$ is anticipated to be a more favorable choice for isotopic analysis.

3.3 Effect of sample gas and sampling depth on oxygen isotopic analysis

Accurate calibration of isotopic mass discrimination is essential for achieving precise isotope ratios with MC-ICP-MS.[53] For the oxygen isotope, the lighter weight and lack of stable isotope pairs as internal standards determine that the standard-sample bracketing (SSB) method can only be used. This method is

simple and convenient to operate; however, a higher level of stability for the instruments is required because the fractionation factor of standard is assumed to be that of sample with this method.[74] The region of stable O isotopic composition can be explored by studying the radial and axial distributions of O ions in the ICP, which can be confirmed by determining the variation of O signal intensity and $^{18}O/^{16}O$ ratio with respect to the position of the torch tube (radial and axial directions) and the sample gas flow rate. It has been established that the radial position of the torch that provides the maximum analyte intensity also results in the most stable isotopic ratios.[75,76] In contrast, the axial position of the torch and sample gas flow rate may not be optimal for both the maximum signal intensity and stable isotopic ratios.[52] The axial distribution of ions in the ICP can be achieved by changing the position of the *Z*-axis of the torch tube (Fig. 5a and c) or the sample gas flow rate (Fig. 5b and d). The *Z*-axis position is the distance from the outer end of the torch tube to the hole of the sampling cone. A more negative *Z*-axis value indicates the plasma is closer to the sample cone. The sample gas flow rate was also manipulated to investigate the effect on ion distribution at the axial position, as a higher flow rate means that the plasma is closer to the sample cone.

For investigation of the *Z*-axis position, as the *Z*-axis position varied from −1.7 mm to 2.0 mm, with the sample gas flow rate remaining constant, the signal intensity of the two analytes initially increased and then decreased, following a similar trend. Comparing the stability of the obtained $^{18}O/^{16}O$ ratio within ±10% of the highest signal intensity, the stability of the $^{18}O/^{16}O$ ratio obtained by measuring $^{18}O^{16}O/^{16}O^{16}O$ (0.002291 ± 0.000001, 2SD) is about 20 times higher than that of $^{18}O/^{16}O$ (0.002222 ± 0.000023, 2SD). To further explore the effect of the sample gas flow rate, the *Z*-position was kept constant, and as the sample gas flow rate increased from 1.0 L min^{-1} to 1.25 L min^{-1}, more ions were extracted into the mass spectrometer, leading to an increase in O intensity. However, the amount of ions extracted is limited by the sample cone diameter[77] and the temperature of the ICP;[78,79] thus, the O signal will not continue to rise indefinitely as the carrier gas flow rate increases. In terms of isotope ratio, the obtained $^{18}O/^{16}O$ by measuring $^{18}O^{16}O/^{16}O^{16}O$ is more stable (0.002289 ± 0.000002, 2SD) than that obtained by measuring $^{18}O/^{16}O$ (0.002251 ± 0.000019, 2SD). Additionally, both the optimum sampling depth and sample gas flow rate for the maximum signal intensity of $^{16}O^{16}O$ can be aligned with the stable area of the isotope ratio, which is superior for tuning and isotopic analysis. Therefore, in terms of isotope ratio stability, compared with the $^{18}O/^{16}O$ ratio, the measured $^{18}O^{16}O/^{16}O^{16}O$ ratio is the preferred choice. And, in practical oxygen isotopic analysis, it is advisable to adjust the sample gas flow rate and the *Z*-axis position to where the maximum signal intensity is achieved.

3.4 Precision and accuracy of oxygen isotopes in oxygen

Analytical precision is dependent on the signal intensity,[52,80] as demonstrated by the exponential function of the precision for the $^{18}O/^{16}O$ isotopic ratios (1 SE) *vs.* the $^{16}O^+$ and $(^{16}O^{16}O)^+$ intensities (Fig. 6a). The internal precision of $^{18}O/^{16}O$ was low when the $(^{16}O^{16}O)^+$ and $^{16}O^+$ signal intensities were less than 100 V. As the signal intensity increases from 100 to 1000 V, there is a rapid improvement in the within-run precision. Therefore, using $(^{16}O^{16}O)^+$ and $^{16}O^+$ signal intensities of more than 1000 V, where the internal precision of $^{18}O/^{16}O$ was better than 1 × 10^7, a 3 × 10^9 Ω resistor was recommended. To obtain long-term

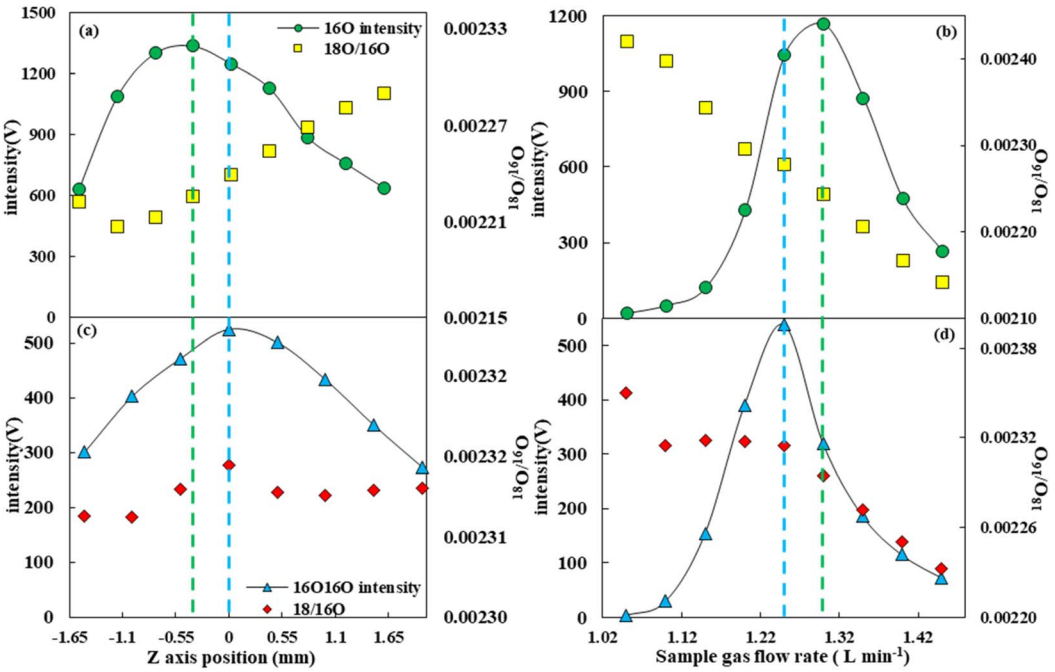

Fig. 5 Relationship between the *Z* position (a and c) and sample gas flow rate (b and d) of $(^{16}O)^+$, $(^{16}O^{16}O)^+$ signal intensity and oxygen isotope ratio ($^{18}O/^{16}O$).

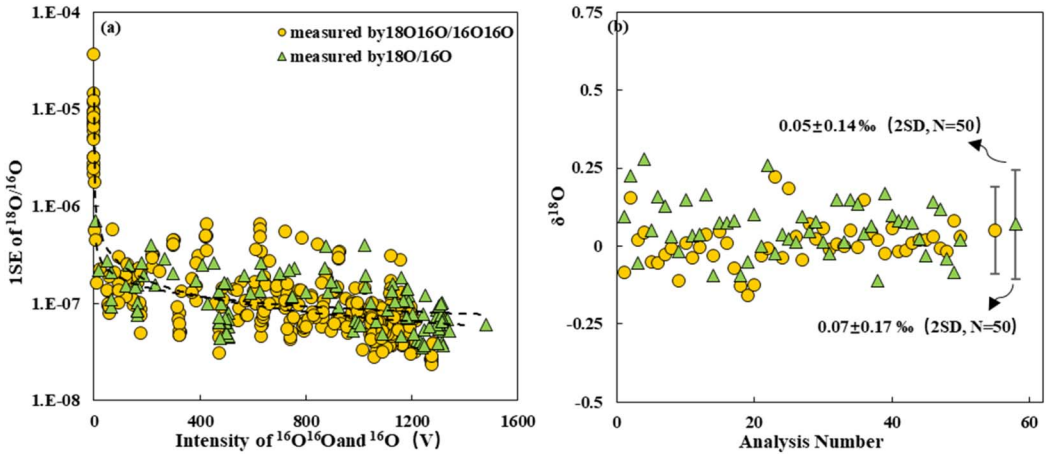

Fig. 6 (a) Relationship between the signal intensity of ^{16}O, ($^{16}O^{16}O$) and the internal precision (1 SE) of $^{18}O/^{16}O$ for oxygen isotopic analysis. (b) Long-term reproducibility of $\delta^{18}O$ by measuring $^{16}O^{18}O/^{16}O^{16}O$ and $^{18}O/^{16}O$.

reproducibility, the $\delta^{18}O$ value was repeatedly measured by analyzing $^{16}O^{18}O/^{16}O^{16}O$ and $^{18}O/^{16}O$ with an optimum O_2 flow rate, respectively. The $\delta^{18}O$ value was repeatedly measured by analyzing $^{16}O^{18}O/^{16}O^{16}O$ and $^{18}O/^{16}O$ with O_2 flow rates of 1.6 and 0.5 mL min^{-1}, sample gas flow rates of 1.254 and 1.285 L min^{-1}, and Z-axis positions of 0.1 and −0.6 mm, respectively, and an RF power of 1050 W. The obtained $\delta^{18}O$ values were 0.05 ± 0.14‰ (2 SD, n = 50) and 0.07 ± 0.17‰ (2 SD, n = 50) for $^{16}O^{18}O/^{16}O^{16}O$ and $^{18}O/^{16}O$, respectively (Fig. 6b), and $^{18}O^{16}O/^{16}O^{16}O$ was preferred.

For the assessment of measurement accuracy of $\delta^{18}O$ using the proposed method, the oxygen isotopes of two different oxygen tanks were analyzed. One oxygen tank was used as the bracketing standard and the other one as the sample. The $\delta^{18}O$ values measured by ^{18}O and ^{16}O were determined at a sample gas flow rate of 1.285 L min^{-1}, an oxygen flow rate of 0.5 ml min^{-1}, and a Z-axis position of −0.6 mm. And the $\delta^{18}O$ values measured by $^{18}O^{16}O$ and $^{16}O^{16}O$ were determined at a sample gas flow rate of 1.254 L min^{-1}, an oxygen flow rate of 1.6 ml min^{-1}, and a Z-axis position of 0.1 mm. The $\delta^{18}O$ values of sample-1 were −0.03 ± 0.22‰ (2 SD, n = 10, measured by ^{18}O and ^{16}O) and 0.16 ± 0.16‰ (2 SD, n = 10, measured by $^{18}O^{16}O$ and $^{16}O^{16}O$). In terms of test accuracy, the accuracy of using $^{18}O^{16}O/^{18}O^{16}O$ to determine the $\delta^{18}O$ value in oxygen was preferred. The obtained values were consistent with those measured according to MAT 253 (0.13 ± 0.1‰; 2 SD, n = 10) and MC-MIP-MS (0.14 ± 0.22‰; 2 SD, n = 6),[81] as shown in Fig. 7, which substantiated the validity of our method.

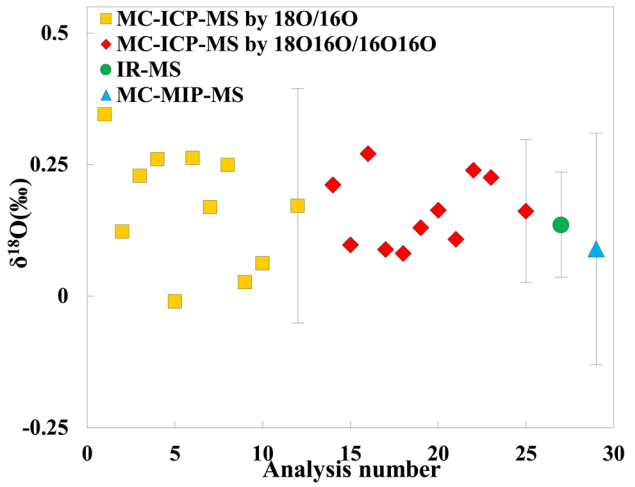

Fig. 7 Measured $\delta^{18}O$ values of oxygen samples using MC-ICP-MS, IR-MS and MC-MIP-MS.

4. Conclusions

Due to the interference from Ar plasma gas, high blank intensity of O from the atmosphere, and the high first ionization energy, no attempt has been made to determine oxygen isotopes by MC-ICP-MS. However, high mass resolution and sub-cup configuration can be used to eliminate the interference of $^{36}Ar^{2+}$ on $^{18}O^{+}$; the application of a 3 × 10^{9} Ω amplifier can be used to obtain the true signal intensity of O blank. Additionally, the applied $^{18}O^{16}O/^{16}O^{16}O$ method can be used to overcome the interference of Ar^{2+} and the ultra-high blank intensity of ^{16}O. Based on the above improvement measures, the obtained long-term reproducibility of $\delta^{18}O$ measured by $^{18}O^{16}O/^{16}O^{16}O$ was better than 0.16‰ (2 SD). The results obtained by MC-ICP-MS were consistent with those measured by IRMS and MC-MIP-MS, which demonstrated that MC-ICP-MS can be used for the accurate determination of oxygen isotopes. It is worth noting that the obtained precision by MC-ICP-MS was worse than that obtained by IRMS, which may be attributed to the high blank. Fortunately, with the use of a shielding gas to maintain positive pressure, preventing atmospheric air from entering the ICP area has been proven to reduce interferences caused by gases such as H, C, N, and O.[82] Using the Atmospheric Interface for Reduced Dust (AIRD) device, optimized through simulations, significantly enhances the analytical capabilities of ICP-MS and effectively manages atmospheric interference. Another reason may be the low ionization rate of O in the Ar-ICP, so the stable He-ICP with high ionization ability may be promising.

Therefore, there is still a long way to go for *in situ* microanalysis of oxygen isotopes using LA-MC-ICP-MS. However, we have already taken the first step to evaluate the capability of MC-ICP-MS to analyze oxygen. Further work will be continued to achieve this goal.

Data availability

The authors declare that the data supporting the findings of this study are available within the paper. Should any raw data files be needed in another format they are available from the corresponding author upon reasonable request. Source data are provided with this paper.

Conflicts of interest

There are no conflicts to declare.

Acknowledgements

This work was funded by the National Natural Science Foundation of China (41927803 and 42473038), MOST (Ministry of Science and Technology) Special Fund from the State Key Laboratory of Geological Processes and Mineral Resources (MSFGPMR01), and the Fundamental Research Funds for the Central Universities, China University of Geosciences (Wuhan).

References

1 J. Hoefs, *Stable Isotope Geochemistry*, Springer International Publishing, Cham, 2015.
2 B. Dhuime, C. J. Hawkesworth, P. A. Cawood and C. D. Storey, *Science*, 2012, **335**, 1334–1336.
3 J. A. Trotter, I. S. Williams, C. R. Barnes, C. Lécuyer and R. S. Nicoll, *Science*, 2008, **321**, 550–554.
4 C. J. Hawkesworth and A. I. S. Kemp, *Nature*, 2006, **443**, 811–817.
5 R. B. Ickert, T. Stachel, R. A. Stern and J. W. Harris, *Geochem. Perspect. Lett.*, 2015, 65–74.
6 D. J. Schulze, B. Harte, J. W. Valley, J. M. Brenan and D. M. D. R. Channer, *Nature*, 2003, **423**, 68–70.
7 J. A. Trotter, I. S. Williams, A. Nicora, M. Mazza and M. Rigo, *Earth Planet. Sci. Lett.*, 2015, **415**, 165–174.
8 U. Ryb and J. M. Eiler, *Proc. Natl. Acad. Sci. U. S. A.*, 2018, **115**, 6602–6607.
9 I. N. Bindeman, A. Bekker and D. O. Zakharov, *Earth Planet. Sci. Lett.*, 2016, **437**, 101–113.
10 U. Wiechert, A. N. Halliday, D.-C. Lee, G. A. Snyder, L. A. Taylor and D. Rumble, *Science*, 2001, **294**, 345–348.
11 R. C. Greenwood, J.-A. Barrat, M. F. Miller, M. Anand, N. Dauphas, I. A. Franchi, P. Sillard and N. A. Starkey, *Sci. Adv.*, 2018, **4**, eaao5928.
12 I. N. Bindeman, D. O. Zakharov, J. Palandri, N. D. Greber, N. Dauphas, G. J. Retallack, A. Hofmann, J. S. Lackey and A. Bekker, *Nature*, 2018, **557**, 545–548.
13 Y.-F. Zheng, B. Fu, B. Gong and L. Li, *Earth-Sci. Rev.*, 2003, **62**, 105–161.
14 G. A. Henkes, B. H. Passey, E. L. Grossman, B. J. Shenton, T. E. Yancey and A. Pérez-Huerta, *Earth Planet. Sci. Lett.*, 2018, **490**, 40–50.
15 Q.-L. Li, X.-H. Li, Y. Liu, G.-Q. Tang, J.-H. Yang and W.-G. Zhu, *J. Anal. At. Spectrom.*, 2010, **25**, 1107–1113.
16 D. Rubatto, B. Putlitz, L. Gauthiez-Putallaz, C. Crépisson, I. S. Buick and Y.-F. Zheng, *Chem. Geol.*, 2014, **380**, 84–96.
17 D. Liu, S. A. Wilde, Y. Wan, S. Wang, J. W. Valley, N. Kita, C. Dong, H. Xie, C. Yang, Y. Zhang and L. Gao, *Chem. Geol.*, 2009, **261**, 140–154.
18 Y. Sun, M. Wiedenbeck, M. M. Joachimski, C. Beier, F. Kemner and C. Weinzierl, *Chem. Geol.*, 2016, **440**, 164–178.
19 A. K. Schmitt, M.-C. Liu and I. E. Kohl, *J. Anal. At. Spectrom.*, 2019, **34**, 561–569.
20 N. M. Ellis and B. H. Passey, *Chem. Geol.*, 2023, **635**, 121616.
21 S. Schmidt, A. Hertwig, A. K. Schmitt, K. Cionoiu, K. D. McKeegan, I. Bindeman, T. D. Rocco and A. Pack, *J. Anal. At. Spectrom.*, 2024, **39**, 439–446.
22 B. Li, M. Wiedenbeck, F. Couffignal, A. M. Álvarez-Valero, H.-M. Bao, C.-F. Fan, J. Han, G.-S. Jin, Y.-B. Peng, M. D. Syczewski, K. T. Tait, F. D. H. Wilke and U. G. Wortmann, *Geostand. Geoanal. Res.*, 2024, **48**, 179–205.
23 R. N. Clayton and T. K. Mayeda, *Geochim. Cosmochim. Acta*, 1963, **27**, 43–52.
24 G. D. Garlick and S. Epstein, *Geochim. Cosmochim. Acta*, 1967, **31**, 181–214.
25 H. P. Taylor Jr and S. Epstein, *Geol. Soc. Am. Bull.*, 1962, **73**, 461–480.
26 D. Elsenheimer and J. W. Valley, *Chem. Geol. Isot. Geosci. Sect.*, 1992, **101**, 21–42.
27 U. Wiechert and J. Hoefs, *Geochim. Cosmochim. Acta*, 1995, **59**, 4093–4101.
28 Z. D. Sharp, *Geochim. Cosmochim. Acta*, 1990, **54**, 1353–1357.
29 D. Elsenheimer and J. W. Valley, *Geochim. Cosmochim. Acta*, 1993, **57**, 3669–3676.
30 D. Mattey, D. Lowry and C. Macpherson, *Earth Planet. Sci. Lett.*, 1994, **128**, 231–241.
31 J. W. Valley, J. R. Chiarenzelli and J. M. McLelland, *Earth Planet. Sci. Lett.*, 1994, **126**, 187–206.
32 S. M. Eggins, R. L. Rudnick and W. F. McDonough, *Earth Planet. Sci. Lett.*, 1998, **154**, 53–71.
33 Z. Li, Z. Hu, Y. Liu, S. Gao, M. Li, K. Zong, H. Chen and S. Hu, *Chem. Geol.*, 2015, **400**, 11–23.
34 H.-R. Kuhn and D. Günther, *J. Anal. At. Spectrom.*, 2004, **19**, 1158–1164.
35 M. Guillong, H.-R. Kuhn and D. Günther, *Spectrochim. Acta, Part B*, 2003, **58**, 211–220.
36 Z. Chen, *J. Anal. At. Spectrom.*, 1999, **14**, 1823–1828.
37 N. T. Kita, T. Ushikubo, B. Fu and J. W. Valley, *Chem. Geol.*, 2009, **264**, 43–57.
38 G.-Q. Tang, X.-H. Li, Q.-L. Li, Y. Liu, X.-X. Ling and Q.-Z. Yin, *J. Anal. At. Spectrom.*, 2015, **30**, 950–956.
39 M. J. Whitehouse and A. A. Nemchin, *Chem. Geol.*, 2009, **261**, 32–42.
40 Q. Yang, X. Xia, W. Zhang, Y. Zhang, B. Xiong, Y. Xu, Q. Wang and G. Wei, *Solid Earth Sci.*, 2018, **3**, 81–86.

41 J. Isa, I. E. Kohl, M.-C. Liu, J. T. Wasson, E. D. Young and K. D. McKeegan, *Chem. Geol.*, 2017, **458**, 14–21.
42 B. Peng, M. He, M. Yang and Y. Shi, *Crystals*, 2023, **13**, 987.
43 F. M. Deegan, M. J. Whitehouse, V. R. Troll, D. A. Budd, C. Harris, H. Geiger and U. Hålenius, *Chem. Geol.*, 2016, **447**, 1–10.
44 B. De Samber, R. De Rycke, M. De Bruyne, M. Kienhuis, L. Sandblad, S. Bohic, P. Cloetens, C. Urban, L. Polerecky and L. Vincze, *Anal. Chim. Acta*, 2020, **1106**, 22–32.
45 S. J. Mojzsis, T. M. Harrison and R. T. Pidgeon, *Nature*, 2001, **409**, 178–181.
46 D. Trail, P. Boehnke, P. S. Savage, M.-C. Liu, M. L. Miller and I. Bindeman, *Proc. Natl. Acad. Sci. U. S. A.*, 2018, **115**, 10287–10292.
47 A. D. Burnham, A. R. Thomson, G. P. Bulanova, S. C. Kohn, C. B. Smith and M. J. Walter, *Earth Planet. Sci. Lett.*, 2015, **432**, 374–380.
48 C. Huang, M. M. Joachimski and Y. Gong, *Earth Planet. Sci. Lett.*, 2018, **495**, 174–184.
49 W. Chen, J. Lu, S.-Y. Jiang, K.-D. Zhao and D.-F. Duan, *Anal. Chem.*, 2017, **89**, 13415–13421.
50 C. Toyama, J.-I. Kimura, Q. Chang, B. S. Vaglarov and J. Kuroda, *J. Anal. At. Spectrom.*, 2015, **30**, 2194–2207.
51 J. Lin, A. Yang, R. Lin, J. Mao, Z. Hu and Y. Liu, *J. Earth Sci.*, 2023, **34**, 1663–1691.
52 J. Lin, Y. Liu, X. Tong, L. Zhu, W. Zhang and Z. Hu, *J. Anal. At. Spectrom.*, 2017, **32**, 834–842.
53 L. Yang, *Mass Spectrom. Rev.*, 2009, **28**, 990–1011.
54 V. Balaram, W. Rahaman and P. Roy, *Geosystems Geoenvironment*, 2022, **1**, 100019.
55 M.-Y. He, L. Deng, J. Liu, Z. dong Jin and T. Ren, *RSC Adv.*, 2023, **13**, 32104–32109.
56 T.-L. Yu, B.-S. Wang, C.-C. Shen, P.-L. Wang, T. F. Yang, G. S. Burr and Y.-G. Chen, *Anal. Chim. Acta*, 2017, **988**, 34–40.
57 Z. Bao, C. Zong, L. Chen, D. Lei, K. Chen and H. Yuan, *J. Anal. At. Spectrom.*, 2018, **33**, 2143–2152.
58 W. Zhang, Z. Hu, Y. Liu, L. Feng and H. Jiang, *Chem. Geol.*, 2019, **522**, 16–25.
59 J. Lin, Y. Liu, Z. Hu, W. Chen, C. Zhang, K. Zhao and X. Jin, *J. Anal. At. Spectrom.*, 2019, **34**, 1145–1153.
60 W. Zhang, Z. Wang, F. Moynier, E. Inglis, S. Tian, M. Li, Y. Liu and Z. Hu, *J. Anal. At. Spectrom.*, 2019, **34**, 1800–1809.
61 I. Gunther-Leopold, B. Wernli, Z. Kopajtic and D. Gunther, *Anal. Bioanal. Chem.*, 2004, **378**, 241–249.
62 E. M. Krupp and O. F. X. Donard, *Int. J. Mass Spectrom.*, 2005, **242**, 233–242.
63 Q. Li, W. Zhang, Z. Hu, Y. Feng, H. Hu, T. Luo, J. Huang and X. Zeng, *Chem. Geol.*, 2023, **636**, 121651.
64 H. Niu and R. S. Houk, *Spectrochim. Acta, Part B*, 1996, **51**, 779–815.
65 C. T. Gerritzen, S. Goderis, H. F. James and C. Snoeck, *Spectrochim. Acta, Part B*, 2024, **217**, 106955.
66 W. Zhang, Z. Hu and Y. Liu, *J. Anal. At. Spectrom.*, 2020, **35**, 1087–1096.
67 J. Fu, Z. Hu, W. Zhang, L. Yang, Y. Liu, M. Li, K. Zong, S. Gao and S. Hu, *Anal. Chim. Acta*, 2016, **911**, 14–26.
68 N. M. Ellis and B. H. Passey, *Chem. Geol.*, 2023, **635**, 121616.
69 N. Dauphas, A. Pourmand and F.-Z. Teng, *Chem. Geol.*, 2009, **267**, 175–184.
70 Y. He, S. Ke, F. Teng, T. Wang, H. Wu, Y. Lu and S. Li, *Geostand. Geoanal. Res.*, 2015, **39**, 341–356.
71 X. Yan, T. Tanaka and H. Kawaguchi, *Appl. Spectrosc.*, 1996, **50**, 182–187.
72 M. Wu, Y. Duan, Q. Jin and G. M. Hieftje, *Spectrochim. Acta, Part B*, 1994, **49**, 137–148.
73 E. V. Polyakova, Yu. N. Nomerotskaya and A. I. Saprykin, *J. Anal. Chem.*, 2020, **75**, 474–478.
74 N. J. Pearson, W. L. Griffin and S. Y. O'Reilly, in *Laser Ablation-ICP-MS In The Earth Sciences*, ed. P. Sylvester, Mineralogical Association of Canada, Québec, 2008, pp. 93–116.
75 H. Andrén, I. Rodushkin, A. Stenberg, D. Malinovsky and D. C. Baxter, *J. Anal. At. Spectrom.*, 2004, **19**, 1217–1224.
76 J. Barling and D. Weis, *J. Anal. At. Spectrom.*, 2012, **27**, 653.
77 M. M. Fraser and D. Beauchemin, *Spectrochim. Acta, Part B*, 2000, **55**, 1705–1731.
78 C. Agatemor and D. Beauchemin, *Anal. Chim. Acta*, 2011, **706**, 66–83.
79 A. A. Mills, J. H. Macedone and P. B. Farnsworth, *Spectrochim. Acta, Part B*, 2006, **61**, 1039–1049.
80 Z. Hu, Y. Liu, S. Gao, W. Liu, W. Zhang, X. Tong, L. Lin, K. Zong, M. Li, H. Chen, L. Zhou and L. Yang, *J. Anal. At. Spectrom.*, 2012, **27**, 1391.
81 J. Lin, Z. Liu, Y. Liu, W. Liu, X. Jiang, G. Zhao, L. Chen and Z. Hu, *Anal. Chem.*, 2023, **95**, 16877–16884.
82 X. Jiang, Y. Liu, W. Liu, J. Lin, Z. Liu, L. Chen, X. Zhu, W. Zhang and Z. Hu, *J. Anal. At. Spectrom.*, 2024, **39**, 2452–2460.

